Soft Matter

Dynamic Article Links ▶

PAPER

Mutual wetting transition between isotropic and anisotropic on directional structures fabricated by femotosecond laser

Dongshi Zhang,[ac] Feng Chen,[*ac] Qing Yang,[*bc] Jinhai Si[ac] and Xun Hou[ac]

This paper reports on the mutual wetting transitions between anisotropic and isotropic on directional structures fabricated by femtosecond (fs) laser. The directional structures are composed of flat Si triangular patterns and fs laser induced spikes. After chemical deposition of a layer of fluoroalkylsilane, the triangular areas and periodic spikes exhibited hydrophobicity and superhydrophobicity, respectively. With increasing water volume, the droplet experienced a series of mutual wetting transitions due to the stick-jump behaviors of triple-phase contact line in orthogonal directions. The typical dynamic triple-phase contact line behaviors were quantitatively analyzed, based on which the specific energy barriers exerted by triangular patterns were speculated. A two-strip model was introduced to explain the reason of mutual wetting transitions.

1. Introduction

Superhydrophobic surfaces have gained increasing interest in both fundamental research and practical applications for their water repellent and self-cleaning properties, such as keeping satellite antenna and radar surfaces clean, preventing contamination or oxidation, reducing hydraulic resistance *etc.* Since the surface wettability is governed by the joint effects of interface chemistry and surface structure, the wetting characteristics of a surface can be enhanced by either hydrophobic coatings or structural engineering. Although hydrophobicity can be enhanced by a chemical modification that lowers the surface energy, contact angles (CAs) larger than 120° have never been achieved for water on flat surfaces.[1] Many techniques have been employed to prepare superhydrophobic surfaces, including lithography,[2] templated electrochemical deposition,[3] wet chemical processes,[4] reactive-ion etching,[5] self-assembly,[6] and laser etching.[7] Among these techniques, microstructuring by femtosecond (fs) laser is particularly attractive for its ability to simultaneously offer dual micro/nanoscale structures simply *via* a one-step process for a wide variety of materials. Therefore, it has been extensively applied to the modulation of surface wettability recently.[8–13]

The superhydrophobic structures include irregular or random obstacles,[14–17] fractal or hierarchical roughness,[18–22] nanorod or nanotube forests,[23–25] and regular patterns.[26–30] The regularly arranged circle[31–34] and square microposts[35–39] have been established as models to investigate how morphologies affect the contact angle (CA) and triple-phase contact line (TPCL). Parallel strips/grooves[40–42] and other structures[43] will elongate a liquid droplet, resulting in different CAs in orthogonal directions, which is known as anisotropy. Anisotropic surfaces are attracting considerable attention for their competence of driving liquid flow along a desired direction, enabling their potential applications in microfluidics and lab-on-chip systems.[44–47]

On anisotropic structures, a droplet will experience a series of dynamic stick-slip/jump behaviors as water volume increases or decreases, which have been analyzed theoretically[48–50] and observed experimentally.[51,52] It is found that such behaviors are attributed to the TPCL pinning/depinning.[53,54] When a droplet advances/recedes, the TPCL will encounter several metastable wells in the energy landscape and get into pinning. Further increase in water volume will lead the droplet overcome the located energy barrier and step into another energy well, hence resulting in the jump behavior and subsequent stick behavior. Inspired by the phenomenon of TPCL pinning-depinning, unidirectional anisotropy has been well controlled by parallel groove/strips structures. Two directional anisotropy is gaining more attention recently. For example, Jokinen *et al.*[55] realized two directional anisotropy in orthogonal directions on hydrophilic triangular structures. However, no one has reported the mutual wetting transitions between anisotropic and isotropic.

In this paper, we present the mutual wetting transitions between anisotropic and isotropic on directional structures consisting of periodical hydrophobic triangular array and superhydrophobic spikes. Through analysis of droplet

aKey Laboratory for Physical Electronics and Devices of the Ministry of Education & Key Laboratory of Photonics Technology for Information, School of Electronics & information Engineering, Xi'an Jiaotong University, 710049, China. E-mail: chenfeng@mail.xjtu.edu.cn; Tel: +86 29-82665105

bState Key Laboratory for Manufacturing Systems Enginnering, Xi'an Jiaotong University, 710049, China

cShaanxi Key Lab of Information Photonic Technique, School of Electronics and Information, Engineering, Xi'an Jiaotong University, Xianning-xilu 28, Xi'an, 710049, China. E-mail: chenfeng @mail.xjtu.edu.cn; yangqing@mail.xjtu.edu.cn

morphologies' variation during the advancing process, the role of triangular patterns in determining wetting transitions was characterized and the dynamic behaviors of TPCL were also depicted. A two-strip model is proposed to explain why droplet transited from anisotropic to isotropic.

Results and discussion

Wetting transitions during advancing motion

Fig. 1(a, c and d) show SEM images of microstructured silicon surface consisting of a periodic triangular array with triangle vertex of 53°. Each triangular pattern is fixed in a square matrix with matrix length equalling to the triangular base length of 500 μm. The fs laser structured region is characterized by tens or hundreds of nm protrusions decorating on self-organized conical spike forests with 10 μm in width and 10 μm in period. The formation of this structure is considered to evolve from the micro-scale ridges.[56] After chemical deposition of a layer of fluoroalkylsilane, periodic spikes exhibited superhydrophobicity with CA almost equal to 180° and sliding angle less than 3°.[57] Fig. 1b shows a wetting transition from anisotropic (0.5 μl) to isotropic (1 μl) on triangular patterns. The difference between CAs measured from Side View ($\theta_\perp$) and Base View ($\theta_\parallel$) was defined as the degree of wetting anisotropy ($\Delta\theta = \theta_\parallel - \theta_\perp$). The view triangles shown in Fig. 1a are also introduced in Fig. 1b to indicate the directions.

Fig. 2. shows the measured CAs, anisotropies and droplet diameters as a function of water drop volume (WDV). For CAs and droplet diameters, both Side View (black) and Base View (red) measurement results are presented for comparison. The first 0.5 μl water drop occupied 1×2 matrixes (the former denotes the triangle quantity of the droplet located observed from Side View; the latter is the quantity observed from Base View). The evident difference of droplet diameter in orthogonal directions indicated that the droplet was in an anisotropic state (Fig. 2c). The anisotropy degree $\Delta\theta$ was 13° (Fig. 2b). An additional 0.5 μl WDV enabled the droplet to overcome the energy barrier exerted by the triangular base angle and compelled subsequent TPCL
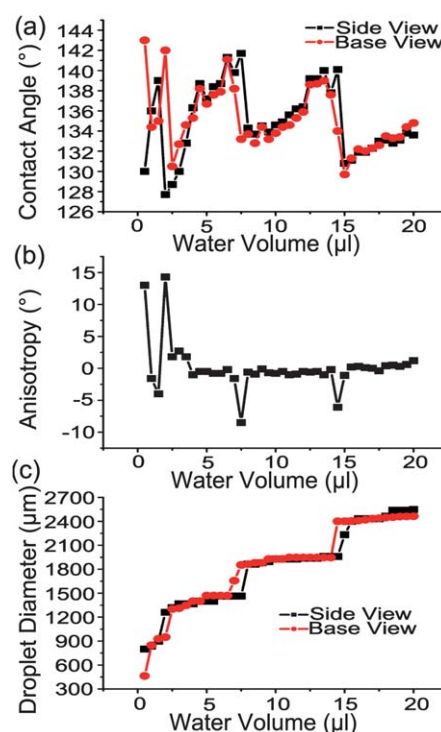
Fig. 2 (a–c) CAs, anisotropies and droplet diameter measured from Side View and Base View.

jump observed from Side View. At this time, the droplet occupied 2×2 matrixes, which indicate that the droplet transited from anisotropic to isotropic. Further increase in WDV would give rise to a series of alternately mutual wetting transitions between isotropic and anisotropic due to the TPCL jump. At WDV = 2 μl, 7.5 μl, 14.5 μl, water droplet transited from isotropic to anisotropic by overcoming the energy barrier of triangular base line. And it would experience reverse wetting transitions at WDV = 2.5 μl, 8 μl, 15 μl by overcoming the energy barriers of triangular base angle and bevel edge, as shown in Fig. 2b.

It is clearly shown that the droplet stabilized around isotropic state for most WDV, only occasionally experiencing the transitions between isotropic and anisotropic, which indicate the directional structures have the ability to draw back the wettability from anisotropic to isotropic. And it is worth pointing out that anisotropy could increase or decrease as WDV increased, distinguishing from traditionally defined anisotropy with $\theta_\perp$ invariably larger than $\theta_\parallel$.[40] It is found that the decrease of anisotropy originated from the TPCL jump observed from Base View. On the contrary, the increase of anisotropy was attributed to the TPCL jump observed from Side View. The occurrence of TPCL jump in one direction was often accompanied by the TPCL stick in another direction.

In addition, the maximal anisotropy degree generally appeared in the initial stage of water dose. The reason is that the same TPCL jump would produce a relatively large change in CAs in the case of small WDV, but a small variation at large WDV.

Triple-phase contact line analysis

Typical TPCL evolutionary process is depicted in Fig. 3. The initial 0.5 μl drop was restricted by 1×2 triangular patterns.
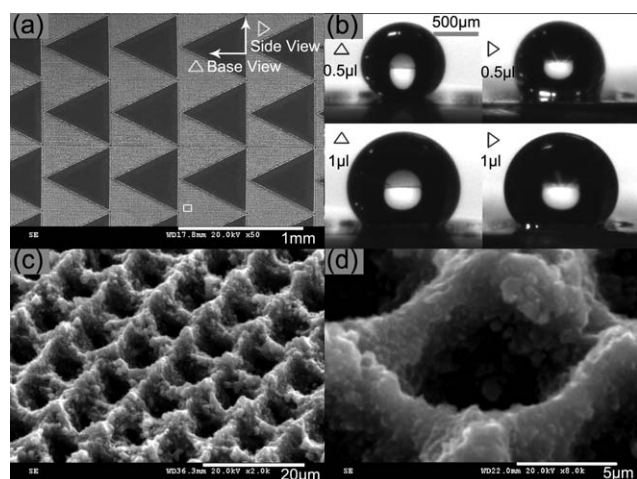

Fig. 1 (a) SEM image of triangular patterns fabricated by femtosecond laser on Si with triangular vertex angle of 53°. (b) water droplet morphologies of 0.5 μl, 1 μl on triangular patterns observed in orthogonal directions. (c, d) large magnification SEM images of the structures irradiated by femtosecond laser.

When the second 0.5 μl water was pumped in, the droplet jumped to the next column of triangular array (Fig. 3a1–a2 and Fig. 1b) and took possession of 2 × 2 matrixes, which led to the wetting transition from anisotropic to isotropic. At WDV = 1.5 μl, the droplet in both directions stuck to the structures (Fig. 3a2). When WDV increased up to 2 μl, the droplet changed from isotropic to anisotropic due to the TPCL jump observed from Side View and TPCL pinning observed from Base View (Fig. 3a2–a3). At WDV = 2.5 μl, the droplet slipped to the base of triangular pattern observed from Side View; meanwhile, the droplet jumped observed from Base View (Fig. 3a3–a4), leading the wettability back to isotropic. At this time, the droplet occupied 3 × 3 matrixes. With WDV increasing from 1.5 μl to 2.5 μl, the droplet advanced in a stick-jump-slip manner observed from Side View, but in a stick-jump manner observed from Base View.

When WDV increased up to 6.5 μl, the droplet maintained stay in 3 × 3 matrixes (Fig. 3b1). At WDV = 7.0 μl, the droplet broke through the energy barrier exerted by the base angle of the middle triangle pattern and jumped a little (Fig. 3b2). And then at WDV = 7.5 μl, the droplet surmounted the energy barriers of the bevel edge upside and jumped to the adjacent triangular patterns, taking possession of 4 × 3 matrixes, thus resulting in the wetting transition from isotropic to anisotropic. In this period, the TPCL moved in a jump-jump manner.

As WDV was further increased, the TPCL jump behaviors followed the trend shown as the red line in Fig. 3c. At WDV = 8.0 μl, the TPCL jumped by overcoming the energy barrier of triangular base line and settled on 4 × 4 matrixes, which led the wettability return to isotropic state. With WDV increasing from 14 μl to 15 μl, the TPCL jumps in orthogonal directions gave rise to another mutual wetting transition between isotropic and anisotropic.

On the basis of TPCL analysis above, as for the droplet advancement observed from Side View, the triangular base line plays the energy barrier role. In this direction, the TPCL may change in two manners: single jump and jump-slip. The bevel edge and the base angle play the energy barrier role observed from Base View. The TPCL may advance in two manners: single jump and jump-jump. The combination of TPCL jump behaviors in orthogonal directions brought about the mutual wetting transitions between anisotropic and isotropic.

To examine the reproducibility and robustness of TPCL, we did a series of experiments on the directional structure. Fig. 4 shows real time record of the water droplets' morphologies in four directions as WDV increased. Fig. 2 revealed that most wetting transitions happened in the initial stage, so here we only concentrate on the wetting response with WDV varying from 0.5 μl to 2.5 μl. The images in the third and fourth row were captured with a light source illumination (SCHOTT KL1500 LCD), which enable us to see the evolutionary process of water droplet morphologies. The decrease of CA indicated the TPCL jump behaviors. It can be seen that the TPCL variation trend in Fig. 4 is the same as that shown in Fig. 3a. The differences are the CAs, which may be attributed to the subtle difference of chemical property or nanostructure over the entire directional surface.

Mechanism analysis

If a water droplet is placed on a hydrophobic substrate with superhydrophobic domains, it tends to wet the hydrophobic domains but to de-wet the superhydrophobic domains. With respect to the directional structures consisting of hydrophobic triangular array and superhydrophobic periodic spikes, increasing WDV would induce a series of mutual transitions between anisotropic and isotropic due to the TPCL jump behaviors. The wetting transitions are attributed to the coexistence of two directional energy barriers for triangular patterns like micropearls,[58] which endow the structures with the capacity to modulate two directional anisotropy. The triangular base line plays the energy barrier role observed from Side View, while the triangular basic angle and bevel edge play the energy barrier role observed from Base View. As WDV increase, the droplet will follow the similar volume-induced wetting trend of parallel strips/grooves.[59–61] That is, the droplet would undergo a series of stick-jump behaviors in orthogonal directions due to the TPCL pinning/depinning by surface defects. A thermodynamic model based on free energy (FE) and free-energy barrier (FEB) has been successfully employed to investigate the superhydrophobic behavior of homogeneous surfaces such as pillar and parallel grooved microstructures.[52] The FE of the drop is given by,[62]
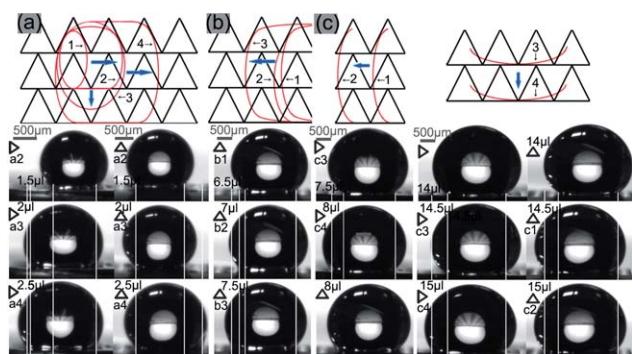

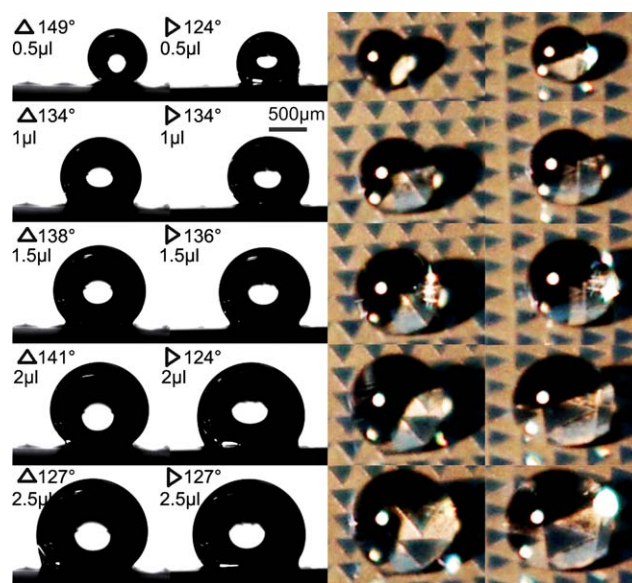**Fig. 3** Series of triple-phase contact line transitions.

Fig. 4 The droplet morphologies' evolutionary process on triangular structures with WDV varying from 0.5 μl to 2.5 μl.
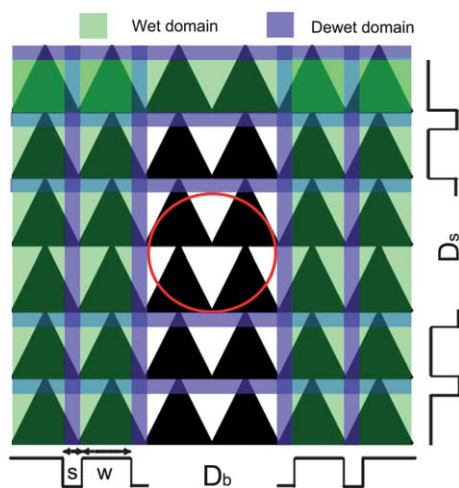
Fig. 5 Two-strip model to simulate the triangular array.

$$f = \frac{F}{\gamma_{lv}} = \frac{d\theta}{\sin\theta} - \int \cos\theta_e(x)dx \qquad (1)$$

where F is the free energy, γ_{lv} is the surface tension between liquid and vapor, d is the droplet diameter, θ is the CA of patterned surface, and θ_e is the intrinsic CA of solid substrate.

In order to understand the reason why the droplet transited from anisotropic to isotropic, a two-strip model is introduced. Considering the coexistence of energy barriers in orthogonal directions, the triangular array is assumed to be parallel strips in orthogonal directions, as demonstrated in Fig. 5. In this figure, the green area denotes the wet domain where droplet would wet and the blue area denotes the de-wet domain where droplet would jump.

In this two-strip model, assuming the droplet initially stays in an isotropic state, as the red circle denotes, the FE in orthogonal directions can be expressed as

$$f_b = \frac{F}{\gamma_{lv}} = \frac{D_b\theta_b}{\sin\theta_b} - D_b\cos\theta_e \qquad (2)$$

$$f_s = \frac{F}{\gamma_{lv}} = \frac{D_s\theta_s}{\sin\theta_s} - D_s\cos\theta_e \qquad (3)$$

where D_b, D_s, θ_b, θ_s are the droplet diameter and CA measured from Base View and Side View, respectively. The CA of the de-wet domain is defined as 180° due to the prominent wetting properties of periodic spikes,[57] while θ_e is the CA of Si substrate that is equal to 110° according to experimental measurement.

Because the droplet is in isotropic state, $D_b \approx D_s$ and $\theta_b \approx \theta_s$, thus $f_b \approx f_s$.

If TPCL jump distance s in one direction breaks the isotropic state to enter adjacent wet domain, the droplet becomes aniso-tropic and the FE correspondingly changes to,

$$f_{b/s} = \frac{F}{\gamma_{lv}} = \frac{(D_{b/s} + s)\theta'_{b/s}}{\sin\theta'_{b/s}} + s - D_{b/s}\cos\theta_e \qquad (4)$$

where $\theta'_{b/s}$ is the CA after jump behavior, s is the jump distance. The jump distance is several hundred microns in our experiments (Fig. 2c), while CA variance is less than 16° (Fig. 2a), which implies the jump distance plays the dominant role in changing FE. It has been recognized that water droplet prefers to spread in the direction with less free energy, so the droplet would then jump back along the direction with less free energy and subse-quently return to isotropic state.[52]

In order to confirm the applicability of this two-strip model, a detailed investigation of CAs after TPCL jump in both direc-tions is carried out using a thermodynamic equation,[63]

$$\theta_A \times L_A/\sin^2\theta_A - L_A^2 \times ctg\theta_A = \theta_B \times L_B/\sin^2\theta_B - L_B^2 \times ctg\theta_B \quad (5)$$

where L_A, L_B, θ_A, θ_B represents the droplet diameter and CA before and just after jump behaviors, respectively. The simulated values θ_{B-c} are listed in Table 1.

It is shown that the largest deviation ($|\theta_B - \theta_{B-c}|$) between experimental CAs and simulated ones is 6°. Taking into account of experimental error ±3° during the CAs measurement, the simulated values θ_{B-c} agree well with our experimental results θ_B, thus proving the validity of the two-strip model.

Experimental

The material was p-doped Si (100) wafers with thickness 0.5 mm. Microstructures were achieved by fs laser in air atmosphere on flat Si surfaces. The details of experimental setup and the scan-ning method were represented by our previous work.[64] The average power used in this experiment was constant of 13 mW, in which case the laser spot size is 12 µm. After the laser irradiation, the samples were cleaned in sequence by ultrasonic bath cleaning in water, acetone and methanol at 40° for 15 min. Afterward, the samples were immersed into fluoroalkylsilane solution with concentration of 2% for two hours to cover a low surface energy organosilane layer, and then its was roasted in a furnace at temperature of 300 °C for another 12 h to make the layer stable and sturdy. The morphology of the surface structures was analyzed with a scanning electron microscopy (SEM). Static CA

Table 1 Contact line length and contact angles in orthogonal directions at transitions points[a]

Direction	L_A/µm	L_B/µm	θ_A(°)	θ_B(°)	θ_{B-c}(°)	$|\theta_B - \theta_{B-c}|$(°)	Volume (µl)
Side View	900	1260	139	127	121	6	1–1.5
	1464	1850	142	134	131	3	7.5–8
	1960	2232	140	131	134	3	14.5–15
Base View	930	1280	142	130	126	4	2–2.5
	1473	1854	141	133	130	3	6.5–7.5
	1968	2367	138	134	129	5	14–14.5

[a] θ_{B-c} – the value calculated from eqn (5).

measurements were performed by a Dataphysics OCA20 CA goniometer with an automated drop dispenser, and image & video capture system, using a sessile drop method. The whole process of drop response were recorded by the videos before the first drop was extruded from the drop dispenser, and ended after the 20 μl water was put on the structure, with 0.5 μl addition at a time and volume speed of 0.5 μl/s. The digital captured drop images from the videos were processed by the image analysis system, which calculated both the left and right CAs from the drop shape with an accuracy of ±0.1°.

Conclusions

In this paper, we reported the volume-induced wetting transitions between anisotropic and isotropic on directional structures which are composed of periodical hydrophobic flat triangular pattern and superhydrophobic spikes. The volume-induced CAs, anisotropies and droplet diameter were investigated. It is found the droplet stabilized around isotropic state for most droplets, only occasionally experiencing the mutual transitions between isotropic and anisotropic, indicating that the directional structure had the ability to pull back the wettability from anisotropic to isotropic. Through analysis of water droplet morphologies in orthogonal directions, the triple-phase contact line (TPCL) jump and subsequent TPCL pinning were found to give rise to the mutual wetting transitions. A two-strip model was proposed to explain the reason of mutual wetting transitions and to predict the contact angles after the TPCL jump. The simulated results were in good agreement with the experimental data.

Acknowledgements

References

1 E. F. Hare, E. G. Shafrin and W. A. Zisman, *J. Phys. Chem.*, 1954, **58**, 236.
2 X. Zhang, F. Shi, J. Niu, Y. G. Jiang and Z. Q. Wang, *J. Mater. Chem.*, 2008, **18**, 621–633.
3 M. Li, J. Zhai, H. Liu, Y. L. Song, L. Jiang and D. B. Zhu, *J. Phys. Chem. B*, 2003, **107**, 9954–9957.
4 M. Li, J. H. Xu and Q. H. Lu, *J. Mater. Chem.*, 2007, **17**, 4772–4776.
5 S. G. Park, J. H. Moon, S. K. Lee, J. Shim and S. M. Yang, *Langmuir*, 2010, **26**, 1468–1472.
6 J. S. Lee, J. Ryu and C. B. Park, *Soft Matter*, 2009, **5**, 2717–2720.
7 R. M. Wagterveld, C. W. J. Berendsen, S. Bouaidat and J. Jonsmann, *Langmuir*, 2006, **22**, 10904–10908.
8 A. Y. Vorobyev and C. L. Guo, *Appl. Phys. Lett.*, 2009, **94**, 224102.
9 Z. K. Wang, H. Y. Zheng, C. P. Lim and Y. C. Lam, *Appl. Phys. Lett.*, 2009, **95**, 111110.
10 T. O. Yoon, H. J. Shin, S. C. Jeoung and Y. I. I. Park, *Opt. Express*, 2008, **16**, 12715–12725.
11 A. M. Kietzig, S. G. Hatzikiriakos and P. Englezos, *Langmuir*, 2009, **25**, 4821–4827.
12 T. Baldacchini, J. E. Carey, M. Zhou and E. Mazur, *Langmuir*, 2006, **22**, 4917–4919.
13 V. Zorba, E. Stratakis, M. Barberoglou, E. Spanakis, P. Tzanetakis, S. H. Anastasiadis and C. Fotakis, *Adv. Mater.*, 2008, **20**, 4049–4054.
14 H. Y. Erbil, A. L. Demirel, Y. Avci and O. Mert, *Science*, 2003, **299**, 1377.
15 M. Miwa, A. Nakajima, A. Fujishima, K. Hashimoto and T. Watanabe, *Langmuir*, 2000, **16**, 5754.
16 Y. Li, L. Li and J. Q. Sun, *Angew. Chem.*, 2010, **122**, 6265–6269.
17 P. Roach, N. J. Shirtcliffe and M. I. Newton, *Soft Matter*, 2008, **4**, 224–240.
18 W. Li and A. Amirfazli, *Soft Matter*, 2008, **4**, 462–466.
19 H. E. Jeong, S. H. Lee, J. K. Kim and K. Y. Suh, *Langmuir*, 2006, **22**, 1640.
20 T. Minami, H. Mayama and K. Tsujii, *J. Phys. Chem. B*, 2008, **112**, 14620–14627.
21 K. Y. Yeh, K. H. Cho and L. J. Chen, *Langmuir*, 2009, **25**, 14187–14194.
22 W. F. Kuan and L. J. Chen, *Nanotechnology*, 2009, **20**, 035605.
23 T. N. Krupenkin, J. A. Taylor, T. M. Schneider and S. Yang, *Langmuir*, 2004, **20**, 3824–3827.
24 J. G. Fan, X. J. Tang and Y. P. Zhao, *Nanotechnology*, 2004, **15**, 501.
25 K. K. S. Lau, J. Bico, K. B. K. Teo, M. Chhowalla, G. A. J. Amaratunga, W. I. Milne, G. H. McKinley and K. K. Gleason, *Nano Lett.*, 2003, **3**, 1701–1705.
26 C. I. Park, H. E. Jeong, S. H. Lee, H. S. Cho and K. Y. Suh, *J. Colloid Interface Sci.*, 2009, **336**, 298–303.
27 Y. K. Kwon, N. Patankar, J. Choi and J. Lee, *Langmuir*, 2009, **25**, 6129–6136.
28 P. Forsberg, F. Nikolajeff and M. Karlsson, *Soft Matter*, 2011, **7**, 104–109.
29 M. J. Xu, N. Lu, H. B. Xu, D. P. Qi, Y. D. Wang, S. L. Shi and L. F. Chi, *Soft Matter*, 2010, **6**, 1438–1443.
30 C. Dorrer and J. Rühe, *Soft Matter*, 2009, **5**, 51–61.
31 L. Barbieri, E. Wagner and P. Hoffmann, *Langmuir*, 2007, **23**, 1723–1734.
32 S. T. Taboryski and R. Larsen, *Langmuir*, 2009, **25**, 1282–1284.
33 T. S. Wong and C. M. Ho, *Langmuir*, 2009, **25**, 12851–12854.
34 M. Callies, Y. Chen, F. Marty, A. Pépin and D. Quéré, *Microelectron. Eng.*, 2005, **78–79**, 100–105.
35 C. Dorrer and J. Rühe, *Langmuir*, 2006, **22**, 7652–7657.
36 C. Dorrer and J. Rühe, *Langmuir*, 2007, **23**, 3179–3183.
37 C. Priest, T. W. J. Albrecht, R. Sedev and J. Ralston, *Langmuir*, 2009, **25**, 5655–5660.
38 A. Shastry, M. J. Case and K. F. Böhringer, *Langmuir*, 2006, **22**, 6161–6167.
39 N. Anantharaju, M. V. Panchagnula, S. Vedantam, S. Neti and S. Tatic-Lucic, *Langmuir*, 2007, **23**, 11673–11676.
40 D. Xia and S. R. J. Brueck, *Nano Lett.*, 2008, **8**, 2819–2824.
41 C. J. Long, J. F. Schumacher and A. B. Brennan, *Langmuir*, 2009, **25**, 12982–12989.
42 O. Bliznyuk, E. Vereshchagina, E. S. Kooij and B. Poelsema, *Phys. Rev. E*, 2009, **79**, 041601.
43 M. K. Kwak, H. E. Jeong, T. Kim, H. Yonn and K. Y. Suh, *Soft Matter*, 2010, **6**, 1849–1857.
44 B. Zhao, J. S. Moore and D. J. Beebe, *Science*, 2001, **291**, 1023–1026.
45 H. Gau, S. Herminghaus, P. Lenz and R. Lipowsky, *Science*, 1999, **283**, 46–49.
46 Y. C. Jung and B. J. Bhushan, *J. Phys.: Condens. Matter*, 2010, **22**, 035104.
47 P. Ball, *Nature*, 1999, **400**, 507–509.
48 S. Brandon, A. Wachs and A. Marmur, *J. Colloid Interface Sci.*, 1997, **191**, 110–116.
49 P. Lenz and R. Lipowsky Phys, *Phys. Rev. Lett.*, 1998, **80**, 1920–1923.
50 J. Leopoldes, A. Dupuis, D. G. Bucknall and J. M. Yeomans, *Langmuir*, 2003, **19**, 9818–9822.
51 N. Anantharaju, M. V. Panchagnula and S. Vedantam, *Langmuir*, 2009, **25**, 7410–7415.
52 X. Y. Zhang and Y. L. Mi, *Langmuir*, 2009, **25**, 3212–3218.
53 R. G. Picknett and R. Bexon, *J. Colloid Interface Sci.*, 1977, **61**, 336–350.
54 G. Pu and S. J. Severtson, *Langmuir*, 2008, **24**, 4685–4692.
55 V. Jokinen, M. Leinikka and S. Franssila, *Adv. Mater.*, 2009, **21**, 4835–4838.
56 M. Y. Shen, C. H. Crouch, J. E. Carey and E. Mazur, *Appl. Phys. Lett.*, 2004, **85**, 5694–5696.
57 F. Chen, D. S. Zhang, Q. Yang, X. H. Wang, B. J. Dai, X. M. Li, X. Q. Hao, Y. C. Ding, J. H. Si and X. Hou, *Langmuir*, 2011, **27**, 359–365.

58 S. Z. Wu, D. Wu, J. Yao, Q. D. Chen, J. N. Wang, L. G. Niu, H. H. Fang and H. B. Sun, *Langmuir*, 2010, **26**, 12012–12016.
59 M. Iwamatsu, *J. Colloid Interface Sci.*, 2006, **297**, 772–777.
60 S. Brandon and A. Marmur, *J. Colloid Interface Sci.*, 1996, **183**, 351–355.
61 S. Brandon, N. Haimovich, E. Yeger and A. Marmur, *J. Colloid Interface Sci.*, 2003, **263**, 237–243.
62 H. Kusumaatmaja and J. M. Yeomans, *Langmuir*, 2007, **23**, 6019–6032.
63 W. Li, Y. P. Diao, H. L. Zhang, G. C. Wang, S. Q. Lu, X. J. Dong, H. B. Dong and Q. L. Sun, *Soft Matter*, 2009, **5**, 2833–2835.
64 D. S. Zhang, F. Chen, G. P. Fang, Q. Yang, D. G. Xie, G. J. Qiao, W. Li, J. H. Si and X. Hou, *J. Micromech. Microeng.*, 2010, **20**, 075029.